environmental microbiology

Environmental Microbiology (2015) **17**(6), 2064–2075 doi:10.1111/1462-2920.12771

Uranium phosphate biomineralization by fungi

Xinjin Liang,[1] Stephen Hillier,[2,3] Helen Pendlowski,[2] Nia Gray,[2] Andrea Ceci[1,4] and Geoffrey Michael Gadd[1,5]*

[1]*Geomicrobiology Group, College of Life Sciences, University of Dundee, Dundee, DD1 5EH, Scotland, UK.*
[2]*The James Hutton Institute, Craigiebuckler, Aberdeen, AB15 8QH, Scotland, UK.*
[3]*Department of Soil and Environment, Swedish University of Agricultural Sciences, Uppsala, Sweden.*
[4]*Laboratorio Biodiversità dei Funghi, Dipartimento di Biologia Ambientale, Sapienza Università di Roma, Rome 00185, Italy.*
[5]*Laboratory of Environmental Pollution and Bioremediation, Xinjiang Institute of Ecology and Geography, Chinese Academy of Sciences, Urumqi 830011, China.*

Summary

Geoactive soil fungi were investigated for phosphatase-mediated uranium precipitation during growth on an organic phosphorus source. *Aspergillus niger* and *Paecilomyces javanicus* were grown on modified Czapek–Dox medium amended with glycerol 2-phosphate (G2P) as sole P source and uranium nitrate. Both organisms showed reduced growth on uranium-containing media but were able to extensively precipitate uranium and phosphorus-containing minerals on hyphal surfaces, and these were identified by X-ray powder diffraction as uranyl phosphate species, including potassium uranyl phosphate hydrate ($KPUO_6.3H_2O$), meta-ankoleite [$(K_{1.7}Ba_{0.2})(UO_2)_2(PO_4)_2.6H_2O$], uranyl phosphate hydrate [$(UO_2)_3(PO_4)_2.4H_2O$], meta-ankoleite ($K(UO_2)(PO_4).3H_2O$), uramphite ($NH_4UO_2PO_4.3H_2O$) and chernikovite [$(H_3O)_2(UO_2)_2(PO_4)_2.6H_2O$]. Some minerals with a morphology similar to bacterial hydrogen uranyl phosphate were detected on *A. niger* biomass. Geochemical modelling confirmed the complexity of uranium speciation, and the presence of meta-ankoleite, uramphite and uranyl phosphate hydrate between pH 3 and 8 closely matched the experimental data, with potassium as the dominant cation. We have therefore demonstrated that fungi can precipitate U-containing phosphate biominerals when grown with an organic source of P, with the hyphal matrix serving to localize the resultant uranium minerals. The findings throw further light on potential fungal roles in U and P biogeochemistry as well as the application of these mechanisms for element recovery or bioremediation.

Received 27 November, 2014; accepted 30 December, 2014. *For correspondence. E-mail g.m.gadd@dundee.ac.uk; Tel. +44 1382 384767; Fax +44 1382 381098.

Introduction

Uranium, which is usually regarded as toxic towards living organisms, is a complex element and able to form a variety of different chemical species in the environment (VanHaverbeke *et al.*, 1996; Suzuki and Banfield, 1999; Gorman-Lewis *et al.*, 2008; Gadd and Fomina, 2011). Microorganisms can have significant roles in uranium biogeochemistry and can influence solubility through sorption, metabolite complexation, nucleation or biomineralization phenomena with redox transformations by prokaryotes in the anaerobic subsurface resulting in reduction of soluble U(VI) (as UO_2^{2+}) to insoluble U(IV) (Lovley and Phillips, 1992; Andres *et al.*, 1993; 1994; Lovley *et al.*, 1993; Macaskie *et al.*, 1994; Yang and Volesky, 1999; Fowle *et al.*, 2000; Gorman-Lewis *et al.*, 2005; Gadd and Fomina, 2011; Ray *et al.*, 2011). Fungi are increasingly appreciated as geoactive agents in the aerobic lithosphere with significant properties depending on their filamentous branching growth habit and chemoorganotrophic metabolism that enable effective colonization and alteration of organic and inorganic substrates, leading to changes in metal mobility and the stability of metal-containing minerals (Gadd, 2007; Gadd and Fomina, 2011; Lloyd and Gadd, 2011). Previous research has demonstrated that fungi exhibit uranium tolerance and can solubilize uranium oxides and depleted uranium and reprecipitate secondary uranium phosphate minerals of the meta-autunite group, uramphite and/or chernikovite, which can encrust fungal hyphae to high accumulation values of 300–400 mg U g dry wt^{-1} (Fomina *et al.*, 2007a,b; 2008). Such minerals appear capable of long-term U retention (Fomina *et al.*, 2007a,b; 2008).

In previous models of uranium phosphate biomineralization by fungi, the contribution of P arising from the action of phosphatase enzymes on P-containing

organic substrates has been hypothesized (Fomina *et al*., 2007a,b; 2008), although direct experimental evidence is lacking. This contrasts with several bacteria where phosphatase-mediated U bioprecipitation has been demonstrated and proposed as a potentially useful approach for treatment of U contamination (Macaskie *et al*., 1992; 1994; 2000; Yong and Macaskie, 1995; 1998; Paterson-Beedle *et al*., 2010; Ray *et al*., 2011; Sivaswamy *et al*., 2011; Kulkarni *et al*., 2013). A *Citrobacter* sp. was demonstrated to accumulate uranyl ions via precipitation with phosphate ligands liberated by phosphatase activity (Macaskie *et al*., 1994; 2000). *Deinococcus radiodurans*, which was genetically engineered to overexpress alkaline phosphatase, was able to precipitate U efficiently over a wide range of U concentrations (Kulkarni *et al*., 2013). Little information exists for the possible role of fungal phosphatase in uranium bioprecipitation (Fomina *et al*., 2007a,b; 2008), although several fungi, including the soil yeast, *Cryptococcus* sp., produce both alkaline and acid phosphatases, and can utilize a number of phosphate sources, including glycerophosphate, p-nitrophenylphosphate, pyrophosphate and phytate (Greenwood and Lewis, 1977; Vogel and Hinnen, 1990; Abd-Alla, 1994; Aleksieva *et al*., 2002). The objective of this research was therefore to investigate a possible role for fungal phosphatase in mediating U bioprecipitation, and we demonstrate for the first time that fungi are capable of precipitating a variety of U-containing phosphate biominerals when grown with an organic source of P, with the hyphal matrix serving to localize the resultant uranium minerals. The findings throw further light on potential fungal roles in U and P biogeochemistry as well as possible significance for element recovery or bioremediation.

Results

Growth rate, tolerance indices and surface pH analysis

In the presence of uranium, growth rates of *Aspergillus niger* and *Paecilomyces javanicus* were reduced, with *P. javanicus* being more sensitive to uranium than *A. niger* (Table 1). Tolerance indices (TI) were used to compare biomass yields of *A. niger* and *P. javanicus* grown on modified Czapek–Dox (MCD) medium with or without 10 mM uranyl nitrate ($UO_2(NO_3)_2$; Table 1). A TI value lower than 100% indicates growth inhibition, while a TI > 100% indicates growth stimulation. The biomass yields of *A. niger* and *P. javanicus* were markedly reduced in the presence of 10 mM uranium (28.0% and 20.6% respectively). The pH value of control medium after growth of *A. niger* was pH 4.3, and pH 7.9 for medium after growth of *P. javanicus*. The final pH value of medium amended with uranyl nitrate after growth of *A. niger* was pH 5.8, while the value for *P. javanicus* grown with uranyl nitrate was pH 6.9.

Table 1. Growth rate, TI and surface pH values of agar underneath growing fungal colonies on uranyl nitrate and glycerophosphate-containing medium.

	$R_u : R_c$	TI %	pH control	pH uranyl nitrate
A. niger	0.6	28	4.3	5.8
P. javanicus	0.4	20.6	7.9	6.9

Growth rate results are presented in the form of ratios of the growth rate on 10 mM uranyl nitrate and 10 mM $C_3H_7Na_2O_6P{\cdot}xH_2O$-amended MCD medium ($R_u$) in relation to growth on control medium with only $C_3H_7Na_2O_6P{\cdot}xH_2O$ (R_c), i.e. $R_u : R_c$. A ratio of 1.0 indicates that the colony extension rate in the presence of uranium (R_u) was the same as the control extension rate (R_c). The control growth rate of *A. niger* grown with $C_3H_7Na_2O_6P{\cdot}xH_2O$ was 4.5 ± 0.1 mm day^{-1} over 20 days incubation at 25°C, that of *P. javanicus* was 4.5 ± 0.1 mm day^{-1} over 48 days incubation at 25°C (average of three replicates ± standard error of the mean). TI values shown are tolerance indices expressed as a percentage derived from the dry biomass weight of colonies grown on MCD medium amended with 10 mM uranyl nitrate and 10 mM $C_3H_7Na_2O_6P{\cdot}xH_2O$. *A. niger* and *P. javanicus* were grown for 30 days and 48 days, respectively, at 25°C in the dark (averages from three measurements are shown with typical relative standard deviations of about 5%). pH values shown are averages from six measurements (with typical relative standard deviations of about 5%) across the agar plates.

Formation of uranium secondary minerals

Both *A. niger* and *P. javanicus* were able to grow at a reduced rate in the presence of 10 mM uranyl nitrate and precipitated secondary minerals (Fig. 1). In contrast to control fungal hyphae from MCD medium (Fig. 1A), platelet-shaped secondary minerals formed along the hyphae of *A. niger* grown with 10 mM uranyl nitrate (Fig. 1B). Some minerals with a morphology similar to hydrogen uranyl phosphate platelets (Suzuki and Banfield, 1999; Paterson-Beedle *et al*., 2010) were also found on biomass of *A. niger* grown with 10 mM uranyl nitrate and 10 mM glycerol 2-phosphate (G2P; Fig. 1C). Similar results were observed for *P. javanicus* on medium amended with 10 mM uranyl nitrate where secondary minerals also formed in association with the fungal hyphae (Fig. 1E and F).

Energy-dispersive X-ray analysis and X-ray mapping

Energy-dispersive X-ray analysis (EDXA) revealed the elemental composition of the secondary minerals found on the fungal hyphae. Compared with control fungal hyphae from MCD medium, which showed only carbon, oxygen, sodium, magnesium, phosphorus and potassium (Fig. 2A), the minerals associated with *A. niger* after growth with uranyl nitrate and G2P showed peaks for

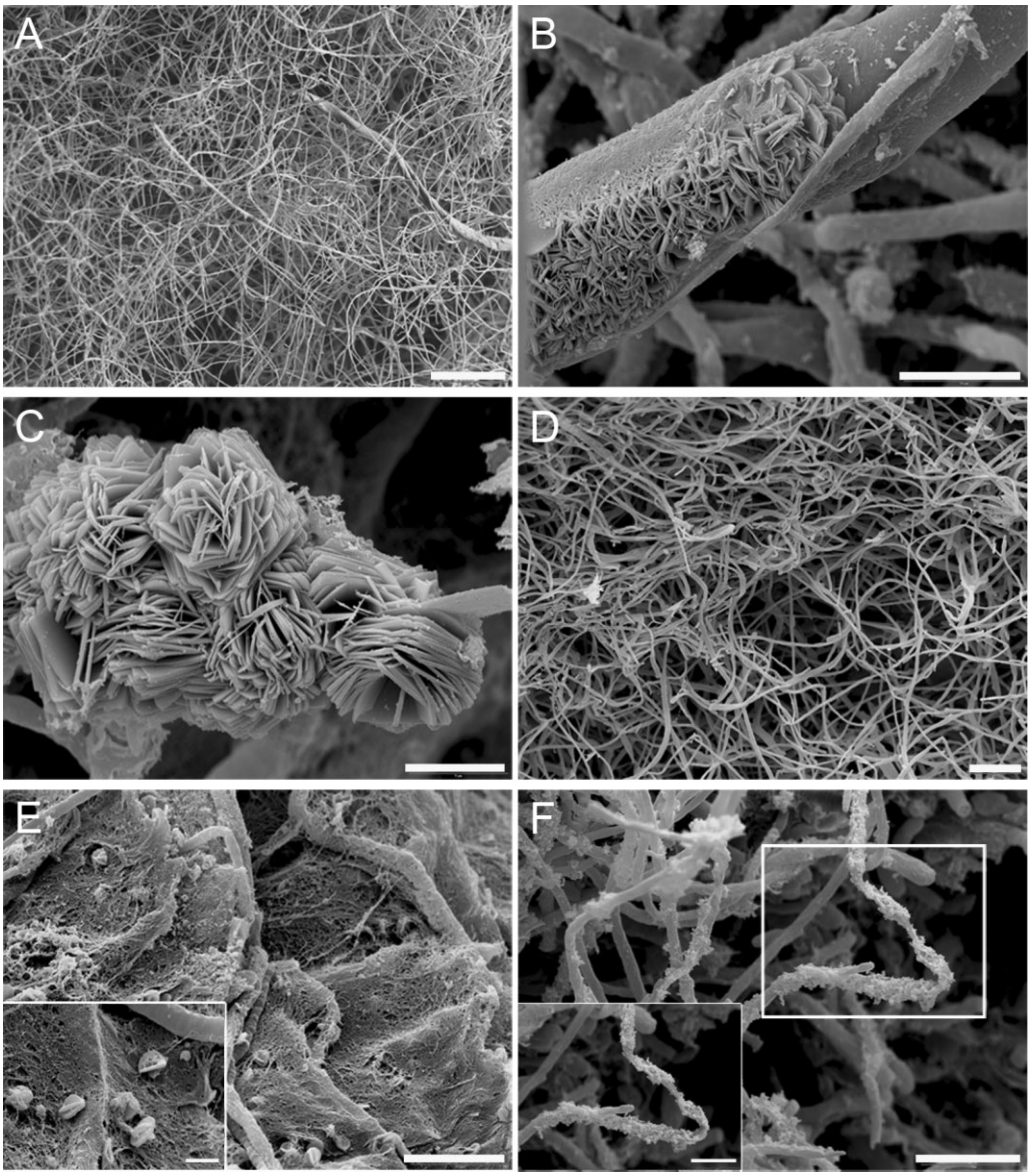

Fig. 1. Scanning electron microscopy of biominerals formed in 10 mM uranyl nitrate and 10 mM $C_3H_7Na_2O_6P{\cdot}xH_2O$-amended MCD medium after fungal growth.
A. Control *A. niger* fungal hyphae grown with 10 mM $C_3H_7Na_2O_6P{\cdot}xH_2O$-amended MCD medium for 30 days at 25°C in the dark, scale bar = 100 μm.
B and C. Biominerals formed in 10 mM uranyl nitrate and 10 mM $C_3H_7Na_2O_6P{\cdot}xH_2O$-amended MCD medium after growth of *A. niger* for 30 days at 25°C in the dark, scale bars: B = 10 μm, C = 5 μm.
D. Control *P. javanicus* fungal hyphae grown with 10 mM $C_3H_7Na_2O_6P{\cdot}xH_2O$-amended MCD medium for 48 days at 25°C in the dark, scale bar = 20 μm.
E and F. Biominerals formed in 10 mM uranyl nitrate and 10 mM $C_3H_7Na_2O_6P{\cdot}xH_2O$-amended MCD medium after growth of *P. javanicus* for 48 days at 25°C in the dark, scale bars: E, F = 10 μm. Insets are higher magnification images of the areas indicated by the squares (scale bars represent 2 and 5 μm respectively). Typical images are shown from several examinations.

carbon, oxygen, sodium, magnesium, phosphorus, potassium and uranium as the main elements detected (Fig. 2B). The minerals showing a druse-like form showed carbon, oxygen, sodium, potassium, phosphorus and uranium (Fig. 2C). Similar EDXA results were obtained for the secondary minerals produced by *P. javanicus* grown with uranyl nitrate and G2P (Fig. 2E and F). X-ray mapping confirmed the elemental location within the secondary minerals (Fig. 3) and showed the presence of carbon (Fig. 3B), oxygen (Fig. 3C), sodium (Fig. 3D), phosphorus (Fig. 3E), potassium (Fig. 3F) and uranium (Fig. 3G) within the secondary minerals produced by *A. niger*. Similar results were obtained for *P. javanicus* (data not shown).

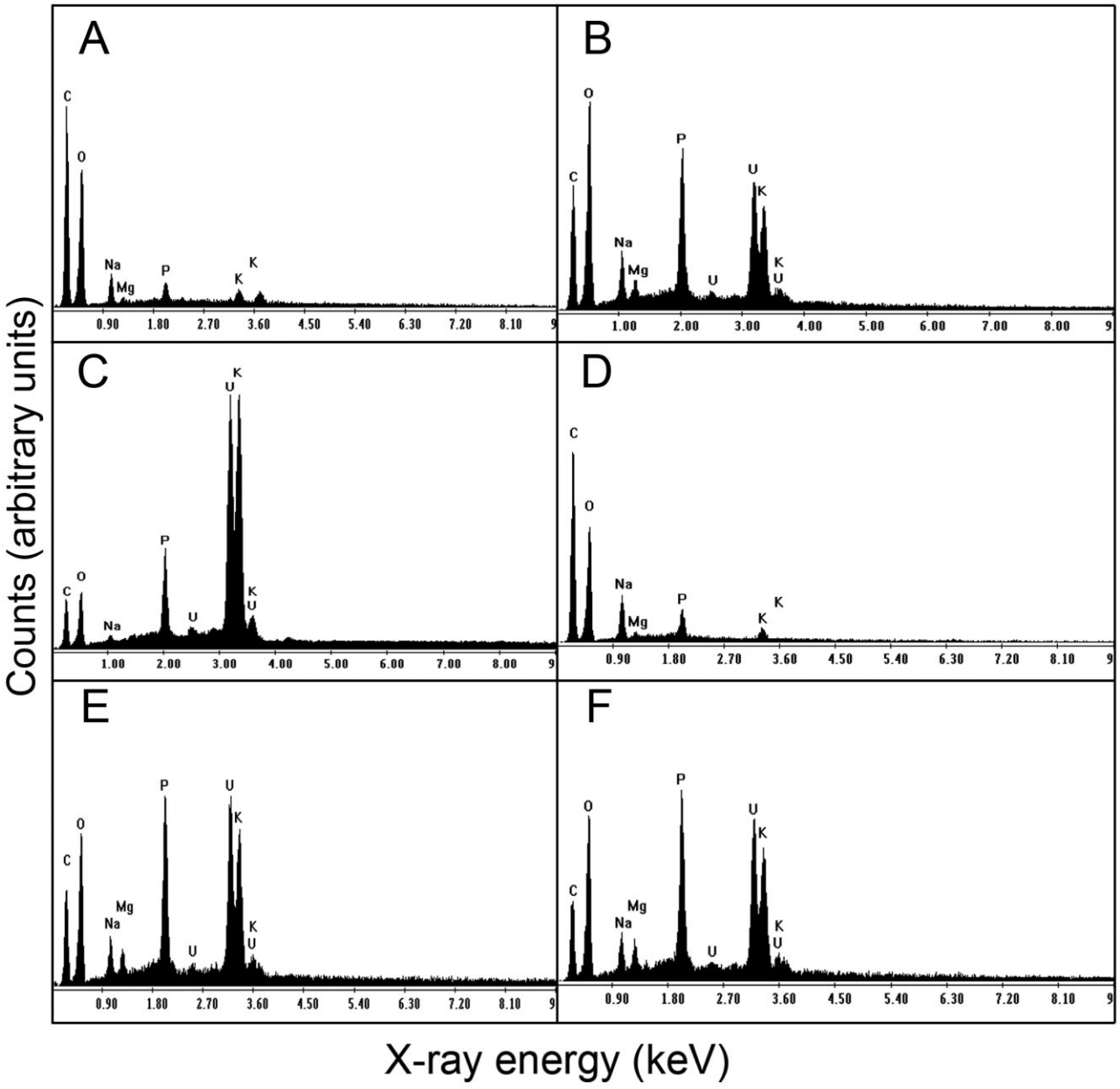

Fig. 2. Energy-dispersive X-ray analysis of fungal hyphae (A, D) grown in control MCD medium amended with G2P only and biominerals produced by fungi during growth with 10 mM uranyl nitrate and 10 mM $C_3H_7Na_2O_6P{\cdot}xH_2O$ (B, C, E, F).
B and C. Uranium-containing biominerals produced by *A. niger* (shown in Fig. 1B and C).
E and F. Uranium-containing biominerals produced by *P. javanicus* (shown in Fig. 1E and F). Typical spectra are shown from one of at least three determinations.

X-ray powder diffraction analysis

The secondary mineral precipitates associated with *A. niger* and *P. javanicus* grown with uranium and glycerophosphate showed the presence of well-crystallized uranyl phosphate compounds matching reference patterns for potassium uranyl phosphate hydrate ($KPUO_6.3H_2O$), meta-ankoleite [$(K_{1.7}Ba_{0.2})(UO_2)_2(PO_4)_2.6H_2O$], uranyl phosphate hydrate [$(UO_2)_3(PO_4)_2.4H_2O$], meta-ankoleite, syn [$K(UO_2)(PO_4).3H_2O$], uramphite, syn ($NH_4UO_2PO_4.3H_2O$) and chernikovite [$(H_3O)_2(UO_2)_2(PO_4)_2.6H_2O$] (Fig. 5). From the diffraction data alone, it is not possible to establish if the precipitates consist of one or some combination of these phases which differ mainly in the cation present in the interlayer site.

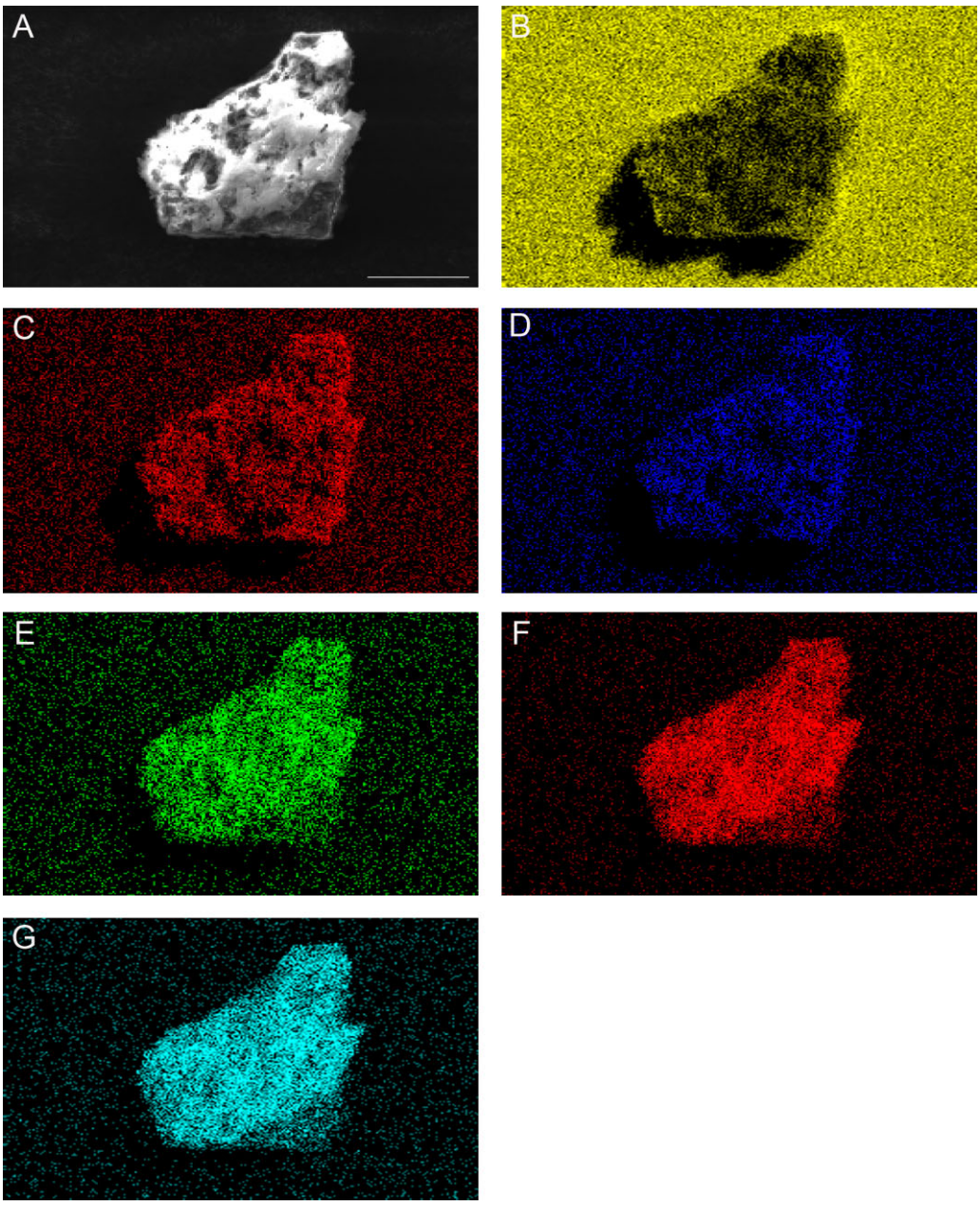

Fig. 3. X-ray mapping of uranium secondary minerals resulting from growth of *A. niger* with $C_3H_7Na_2O_6P{\cdot}xH_2O$ and uranium. X-ray maps of the uranium secondary minerals were obtained using a Philips XL30 ESEM operating at an accelerating voltage of 20 kV.
A. Environmental scanning electron microscope image of uranium minerals (in the absence of any Au/Pd coating). Energy-dispersive X-ray analysis confirmed the presence of (B) carbon, (C) oxygen, (D) sodium, (E) phosphorus, (F) potassium and (G) uranium (scale bar = 50 μm). Typical maps are shown from one of several determinations.

Geochemical modelling

Multiple geochemical equilibria between water, complexes, ion exchangers, minerals, solid solutions, gases and surface complexes can be performed using PHREEQC (Smith *et al.*, 2001; Charlton and Parkhurst, 2011; Parkhurst and Appelo, 2013), and this software was used to generate a diagram of uranium speciation for bioprecipitation of uranium phosphate minerals mediated by fungal species. Uranium in the environment tends to form yellow uranyl(VI) compounds and in the presence of phosphate, uranyl ions rapidly form insoluble orthophosphate, while in the absence of phosphate, uranyl(VI) speciation is driven by interactions with water and carbonate in aqueous systems (Kalin *et al.*, 2004). The diagram shows the mineral species of uranium that

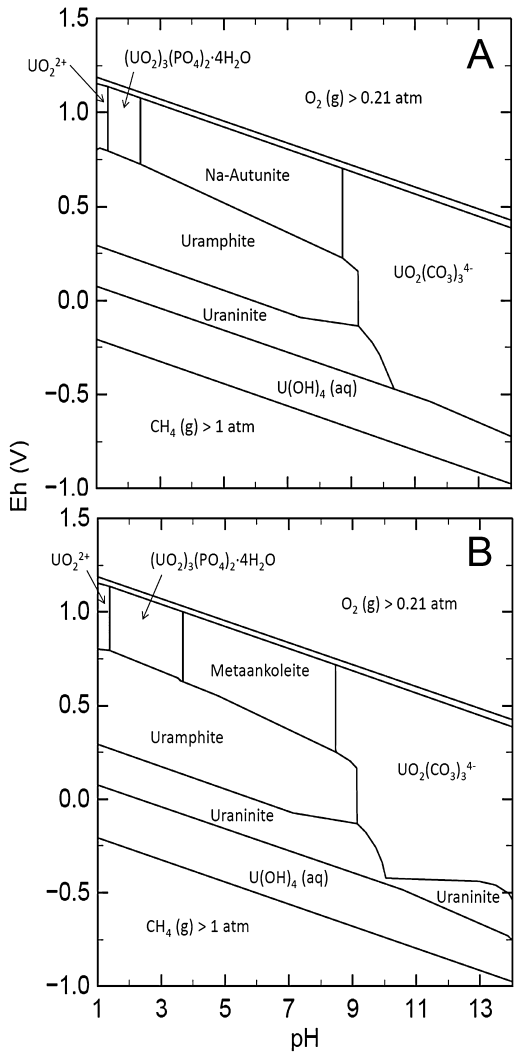

Fig. 4. Distribution of U-species complexes and U minerals for the system H-O-C-P-U-Mg-S-K-Na-N-Fe-Cl, with 10 mM uranyl nitrate and 10 mM $C_3H_7Na_2O_6P{\cdot}xH_2O$-amended MCD medium after fungal growth at 25°C. A is where sodium is assumed to be the dominant cation in the system and B is where potassium is assumed to be the dominant cation. It is assumed that organic phosphate has been hydrolysed by phosphatase activity and is present as inorganic phosphate in solution.

are theoretically dominant in the tested conditions with MCD medium (Fig. 4A and B). The data were calculated for a temperature of 25°C and total dissolved uranium in the presence of dissolved chloride, carbonate, nitrate and sulphate, with sodium (Fig. 4A) or potassium (Fig. 4B) as the main cations, since they are components of MCD medium. At given physico-chemical conditions of pH and E_h, several U species may occur in the aqueous system, and this influences the resulting complexation reactions. The diagram indicates that UO_2^{2+}, $(UO_2)_3(PO_4)_2.4H_2O$, uramphite, $U(OH)_4$ and uraninite dominate the aqueous speciation of uranium at pH values < 9 for both simulations, while meta-ankoleite dominates the pH range from 4 to 9 with potassium as the main cation (Fig. 4B). In contrast, with sodium as the main cation, Na-autunite occupies the pH range 3 to 9 at the higher E_h conditions (Fig. 4A). At higher pH values, the speciation of U(VI) is dominated by a series of strong aqueous carbonate complexes ($UO_2(CO_3)_3^{4-}$) for both conditions which increases the solubility of uranium and therefore decreases uranyl adsorption to surfaces (Fig. 4A and B). The presence of meta-ankoleite, uramphite and $(UO_2)_3PO_4.4H_2O$ between pH 3 and 8 closely matches the X-ray powder diffraction (XRPD) data which confirms that the theoretical simulation with potassium as the dominant cation agrees with the findings from the experimental system. Under reducing conditions, due to the extreme affinity of U(IV) for oxygen, large groups of oxyhydrates, uranyl hydroxides and urinates tend to form, and U(IV) speciation is dominated by $U(OH)_{4(aq)}$ when the E_h is < 0 in the presence of dissolved chloride, nitrate, carbonate and sulfate (Fig. 4A and B). It is important to note that the concentration of uranium strongly affects the formation of the different uranium species, while aqueous U complexes also undergo protonation or deprotonation reactions together with polymerization to form various aqueous species of uranium (VanHaverbeke *et al*., 1996; Suzuki and Banfield, 1999; Yang and Volesky, 1999; Gorman-Lewis *et al*., 2008; Gadd and Fomina, 2011). Conditional solubility product constant (K_{sp}) values can be used to yield rough approximations of solubility behaviour and the relative stabilities of the U secondary minerals under environmentally relevant conditions: the higher the K_{sp}, the more soluble is the compound (Guibal *et al*., 1995). Table 2 lists the reactions and corresponding K_{sp} values of the uranium mineral phases which are relevant to this study. For example, when comparing potassium uranyl phosphate hydrate (log K_{sp} –26.28) (Markovic and Pavkovic, 1983), meta-ankoleite (log K_{sp} –24.30) (VanHaverbeke *et al*., 1996) and uramphite (log K_{sp} –26.50) (Markovic *et al*., 1988), the log K_{sp} for uranyl phosphate hydrate (–49.00) (Markovic and Pavkovic, 1983) is much smaller indicating that its solubility is lower than the other uranyl species in the system (Table 2).

Discussion

Because of their extremely low solubilities under circumneutral pH conditions, uranyl phosphates are an extremely important group of uranyl mineral phases for controlling U mobility in the environment (Markovic *et al*., 1988; Gorman-Lewis *et al*., 2005; Paterson-Beedle *et al*., 2010). In addition, the formation of insoluble uranium phosphates is of relevance to bioremediation of contaminated soil and liquid wastes, and this can be mediated by bacteria and fungi (Macaskie *et al*., 1992; 1994; 2000;

Table 2. Composition, dissolution reactions and associated solubility products of representative uranyl phosphate minerals.

Mineral phase	Composition	Reaction	log K_{sp} (I = 0)	References
Potassium uranyl phosphate hydrate	$KPUO_6{\cdot}3H_2O$	$KPUO_6{\cdot}3H_2O \rightleftharpoons K^+ + UO_2^{2+} + PO_4^{3-} + 3H_2O$	−26.28 (± 0.25)	(Markovic and Pavkovic, 1983)
Meta-ankoleite, syn	$K(UO_2)(PO_4){\cdot}3H_2O$	$KUO_2PO_4{\cdot}3H_2O \rightleftharpoons K^+ + UO_2^{2+} + PO_4^{3-} + 3H_2O$	−24.30 (± 0.81)	(VanHaverbeke *et al.*, 1996)
Uranyl phosphate hydrate	$(UO_2)_3(PO_4)_2{\cdot}4H_2O$	$(UO_2)_3(PO_4)_2{\cdot}3H_2O \rightleftharpoons 3UO_2^{2+} + 2PO_4^{3-} + 4H_2O$	−49.00 (± 0.80)	(Markovic and Pavkovic, 1983)
Uramphite	$NH_4UO_2PO_4{\cdot}3H_2O$	$NH_4UO_2PO_4{\cdot}3H_2O \rightleftharpoons NH_4^+ + UO_2^{2+} + PO_4^{3-} + 3H_2O$	−26.50 (± 0.09)	(Markovic *et al.*, 1988)

Yong and Macaskie, 1995; Fomina *et al.*, 2007a,b; 2008; Paterson-Beedle *et al.*, 2010; Gadd and Fomina, 2011). The first detailed evidence for fungal transformation of uranium solids revealed that saprotrophic, ericoid and ectomycorrhizal fungi could solubilize the uranium oxides UO_3 and U_3O_8 and accumulate large amounts of uranium (> 80 mg U g dry wt^{-1}) within the mycelium, most of which was biomineralized as well-crystallized uranium phosphate minerals of the meta-autunite group (Fomina *et al.*, 2007a). There was a strong correlation with oxalate excretion and total U accumulation in colonies grown on uranium oxide-containing media (Fomina *et al.*, 2007a) and crystalline and amorphous uranium phosphate precipitated on hyphal surfaces within the mycelial microenvironment (Fomina *et al.*, 2007a). Subsequent research showed that ammunition depleted uranium (DU) could also be transformed and biomineralized by fungi with extensive polycrystalline precipitates (up to 300–400 mg U g dry wt^{-1}) covering hyphae and cord-like aggregates in which U was coordinated with P as U-O-P linkages (Fomina *et al.*, 2008). The crystalline precipitates of U arising from growth on DU were identified as the meta-autunite group minerals uramphite and/or chernikovite (Fomina *et al.*, 2008). The mechanism of uranium phosphate biomineralization was not established although it was hypothesized that available phosphate ligands could arise from the action of fungal acid phosphatases on organic P-containing substrates (Fomina *et al.*, 2008). The ability of fungi to release P from inorganic sources is well known, this ability being a ubiquitously found property especially in mycorrhizal fungi (Gadd, 2007; 2010), and such release can result in the formation of secondary mycogenic metal phosphates (Fomina *et al.*, 2007a,b; 2008; Gadd, 2010; Rhee *et al.*, 2012; 2014a,b). This has been shown for lead where fungal biodeterioration can result in pyromorphite ($Pb_5[PO_4]_3X$ [X = F,Cl or OH]) formation (Rhee *et al.*, 2012; 2014a,b). However, the significance of organic P substrates as a source of P has not been established. This is an important question since P is a major elemental constituent of living organisms, and organic P contributes significantly to the total pool of P in the terrestrial environment through biomass degradation and excreted products (Yadav and Tarafdar, 2003; Gadd, 2004; Paterson-Beedle *et al.*, 2010).

In this study, the soil fungi *A. niger* and *P. javanicus* were found to be able to form uranyl phosphate secondary biominerals when grown in the presence of soluble uranium nitrate and glycerol 2-phosphate. Secondary uranium minerals developed on hyphal surfaces within the mycelial system, and were identified as hydrated uranyl phosphate species. Some variations may occur through incorporation of potassium ($KPUO_6.3H_2O$, $(K_{1.7}Ba_{0.2})(UO_2)_2(PO_4)_2.6H_2O$, $K(UO_2)(PO_4).3H_2O$, or ammonium ($NH_4UO_2PO_4.3H_2O$) present in the growth medium. There was no detection of Na-autunite by XRPD even with the relatively large amount of sodium present in the MCD medium which might due to competition between potassium and sodium. Thus, the possibility of other uranyl phosphate minerals being formed by fungi with the same pattern of bioprecipitation cannot be ruled out. The presence of acid phosphatases in fungi is well known (Gibson and Mitchell, 2005; George *et al.*, 2007; Aseri *et al.*, 2009; Rajeshkumar and Ilyas, 2011; Newsome *et al.*, 2014), and we can conclude that uranium phosphate bioprecipitation is a result of phosphatase-mediated P release from the organic substrate, since no other P source was present in the experimental system. Phosphatase-mediate uranium phosphate bioprecipitation has been clearly demonstrated in a *Serratia* sp., where uranium precipitation as a result of G2P hydrolysis and release of HPO_4^{2-} by a metal-resistant acid phosphatase resulted in deposition of $UHPO_4$ on the cells (Macaskie *et al.*, 1992; 1994; 2000; Bonthrone *et al.*, 1996; Paterson-Beedle *et al.*, 2010). In related studies with a phytase-producing *Escherichia coli* that can hydrolyse phytic acid-releasing phosphate, $UO_2HPO_4.4H_2O$ was precipitated within immobilized cell bioreactors (Paterson-Beedle *et al.*, 2010). The crystalline form of the bacterial uranium phosphate produced showed very close similarity to the mycogenic uranium phosphate crystals observed in this study (Fig. 1C). This bioprecipitation of uranium is likely to be preceded by physico-chemical processes such as adsorption, surface

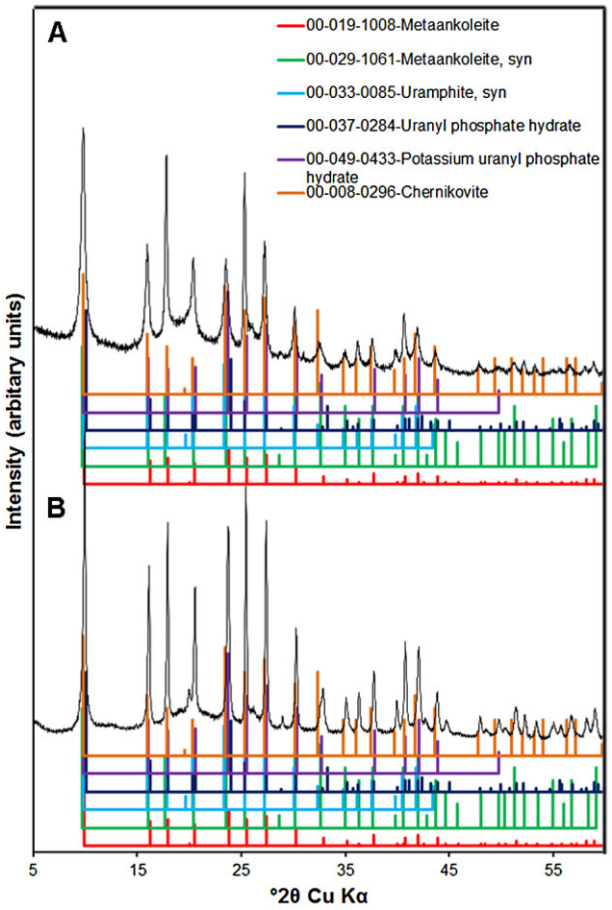

Fig. 5. X-ray powder diffraction patterns of biominerals extracted from 10 mM uranyl nitrate and 10 mM $C_3H_7Na_2O_6P{\cdot}xH_2O$-amended MCD medium after fungal growth at 25°C in the dark. Patterns for dominant mineralogical components are shown, as well as the new biominerals produced as a result of fungal activity: potassium uranyl phosphate hydrate ($KPUO_6{\cdot}3H_2O$), meta-ankoleite ($(K_{1.7}Ba_{0.2})(UO_2)_2(PO_4)_2{\cdot}6H_2O$), uranyl phosphate hydrate ($(UO_2)_3PO_4{\cdot}4H_2O$), meta-ankoleite, syn ($K(UO_2)(PO_4){\cdot}3H_2O$), uramphite, syn ($NH_4UO_2PO_4{\cdot}3H_2O$) and chernikovite ($(H_3O)_2(UO_2)_2(PO_4)_2{\cdot}6(H_2O)$). X-ray powder diffraction patterns were collected from mineral particulates harvested from uranyl nitrate and $C_3H_7Na_2O_6P{\cdot}xH_2O$-amended MCD medium after (A) growth of *A. niger* and (B) *P. javanicus* for 30 and 48 days, respectively, at 25°C. Typical patterns are shown from one of several determinations.
A. X-ray powder diffraction pattern collected from mineral particulates harvested from 10 mM uranyl nitrate and 10 mM $C_3H_7Na_2O_6P{\cdot}xH_2O$-amended MCD medium after growth of *A. niger* for 30 days at 25°C in the dark.
B. X-ray powder diffraction pattern collected from mineral particulates harvested from 10 mM uranyl nitrate and 10 mM $C_3H_7Na_2O_6P{\cdot}xH_2O$-amended MCD medium after growth of *P. javanicus* for 48 days at 25°C in the dark.

complexation and ion exchange at hyphal surfaces (Fomina *et al.*, 2008). Fungal and bacterial cell walls and outer surfaces contain many functional groups, and the ability to strongly biosorb soluble uranium species has been documented widely (Krueger *et al.*, 1993; Guibal *et al.*, 1995; Fowle *et al.*, 2000; Macaskie *et al.*, 2000; Francis *et al.*, 2004; Gorman-Lewis *et al.*, 2005).

The uranyl ion is very stable and can form a variety of chemical complexes. The relationship between different complexing agents, pH and the solubility of the different uranium minerals is very complex (Fig. 4). Geochemical modelling greatly assisted interpretation of our findings, and showed that under acidic conditions, the phosphate species HPO_4^{2-} and $H_2PO_4^-$ combined with mobile uranium to generate the uranium phosphates $UO_2HPO_4.4H_2O$, $UO_2(HPO_4)_2^{2-}$ and $U(HPO_4)_4^{4-}$. Hydroxide complexes, such as UO_2OH^+, $(UO_2)_2(OH)_2^{2+}$, $(UO_2)_3(OH)_5^+$ and $(UO_2)_3(OH)_7^-$, tend to form under near neutral conditions (Fig. 4). Under alkaline conditions, the dominant uranium species are carbonate complexes together with available hydroxyl, carbonate or phosphate ligands in the system (Fig. 4). Generally, the form of uranyl phosphate precipitation is $M(UO_2PO_4)_n{\cdot}xH_2O$, where M can be a monovalent or divalent cation depending on the cations present in the system and their solubilities, while n can be 1 or 2 depending on the uranium valence state and the metal cations present (Gorman-Lewis *et al.*, 2008). This can explain the formation of potassium uranyl phosphate rather than sodium uranyl phosphate. Previous work on uranium phosphate precipitation by bacteria has demonstrated the formation of autunites with a structure of negatively charged layers of $(UO_2PO_4)_n$ separated by staggered layers of water molecules and compensating cations (Yong and Macaskie, 1995; 1998). This can also explain the formation of the different uranyl phosphate phases identified in this study (Fig. 5). The pH-dependent speciation, dissolution reactions and associated solubility of uranium and uranyl phosphate minerals in soils and aqueous systems has been previously documented (Markovic and Pavkovic, 1983; VanHaverbeke *et al.*, 1996; Fomina *et al.*, 2007b; Gorman-Lewis *et al.*, 2008). The E_h-pH diagram confirms the geochemical model of uranium speciation in our experimental system with an organic phosphate source as the sole phosphorus source. It should be emphasized that XRPD does not identify the potassium uranyl phosphates unequivocally as a variety of uranyl phosphates can have almost identical XRPD patterns. The XRPD data only indicates that some form of (X) uranyl phosphate is present where X, depending on the chemistry of the reaction medium, could be, e.g. Mg, K, Na, H, Fe, NH_4 or a mixture of these cations. However, even with possible interference from organic acid secretion, such as oxalate (Fomina *et al.*, 2007a,b; 2008), our findings demonstrate that uranyl phosphate formation mediated by fungal phosphatase activity and subsequent interactions with the biomass were most important in uranium bioprecipitation (Fig. 6).

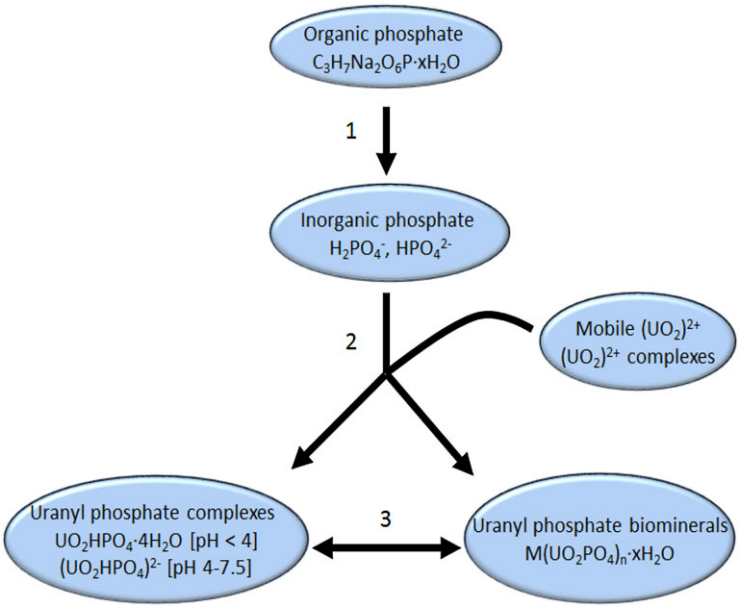

Fig. 6. The role of fungal phosphatases in uranium bioprecipitation. (i) Fungal phosphatase hydrolyses organic phosphate and releases inorganic phosphate (e.g. $H_2PO_4^-$ and HPO_4^{2-}) which can (ii) react with mobile uranium species (e.g. $(UO_2)^{2+}$ and $(UO_2)^{2+}$ complexes) to form inorganic uranyl phosphate complexes and precipitates (e.g. $UO_2HPO_4{\cdot}4H_2O$, $(UO_2HPO_4)^{2-}$). The accumulation of inorganic uranyl phosphate complexes and reaction with functional groups on the fungal biomass leads to (iii) extensive uranyl phosphate biomineralization eventually forming crystalline $M(UO_2PO_4)_n{\cdot}xH_2O$ minerals (where M is a monovalent or divalent cation, e.g. K).

Our proposed model of the role of fungal phosphatases in uranium bioprecipitation describes, for the first time, the formation of crystalline meta-autunite minerals on fungal mycelia grown in the presence of uranyl nitrate and glycerol 2-phosphate as sole phosphorus source (Fig. 6). Some previous research has suggested overproduction of an acid-type phosphatase can occur as a toxic metal immobilization or detoxification mechanism for fungi (Guibal *et al*., 1995; Gibson and Mitchell, 2005). From this study, it is clear that fungal phosphatase activity is involved in uranium bioprecipitation in conjunction with the physico-chemical properties of hyphal surfaces and extracellular polymeric substances, which can serve as matrices for uranium diffusion, complexation and precipitation (Fig. 6). In conclusion, this work is the first demonstration of fungal bioprecipitation of uranium phosphates when growing with an organic phosphorus source, and provides further understanding of fungal roles in the biogeochemical uranium and phosphorus cycle and possible directions of research in relation to biomineralization mechanisms for uranium bioremediation.

Experimental procedures

Organisms and media

Experimental fungi used were *Aspergillus niger* van Tieghem (ATCC 201373) and *Paecilomyces javanicus* (Friedrichs and Bally) A.H.S. Brown and G. Smith. The fungal species selected have been previously demonstrated to be efficient in mineral dissolution and toxic metal transformations (Fomina *et al*., 2007a,b; 2008; Gadd, 2010; Rhee *et al*., 2012; 2014a,b; Wei *et al*., 2013). The fungi were routinely maintained on 20 cm^3 modified MCD amended with 10 mM glycerol 2-phosphate disodium salt hydrate ($C_3H_7Na_2O_6P{\cdot}xH_2O$) (G2P), as sole P source, in 90 mM diameter Petri dishes and grown at 25°C in the dark. *A. niger* was grown for 4 days, while *P. javanicus* was grown for 10 days prior to experimental subculture. Modified Czapek–Dox medium consists of (l^{-1} Milli-Q water): glucose 3 g, $NaNO_3$ 3 g, $Mg(NO_3)_2{\cdot}6H_2O$ 0.5 g, KCl 0.5 g, $Fe(NO_3)_3{\cdot}9H_2O$ 0.01 g and agar No. 1 (Lab M, Bury, UK) 20 g. Uranyl nitrate and G2P were dissolved separately in Milli-Q water and sterilized by membrane filtration (cellulose nitrate, 0.2 µm pore diameter, Whatman, Maidstone, Kent, UK) and added to autoclaved MCD medium (121°C, 15 min) to give a 10 mM final concentration, at a temperature of around 50°C prior to pouring. After autoclaving and cooling to around 50°C, the medium was adjusted to pH 6 using sterile 1 M NaOH. Ninety-mm diameter dialysis membranes (Focus Packaging and Design Ltd, Louth, UK) were sterilized by autoclaving three times (121°C, 15 min) in Milli-Q water, and were used to cover agar and separate the fungus from the medium but still allow the colony access to diffusible nutrients. Inocula consisted of a 5 mM diameter core cut from the margins of an actively growing fungal colony using a sterile cork borer (autoclaved at 121°C for 15 min) and placed in the centre of the Petri dish and incubated at 25°C in the dark. All experiments were conducted at least in triplicate.

Growth, toxicity assessment and pH analysis

Colony expansion was measured daily in two directions for each fungal colony until the colonies either had reached the edge of the Petri dish or showed no further growth. Fungal biomass was removed from the dialysis membranes using a sterile scalpel, and dried to constant weight in a vacuum desiccator at room temperature for at least 30 days. Uranium tolerance was evaluated using a TI as follows: (dry weight of U-exposed mycelium/dry weight of control mycelium x 100%) (Wei *et al*., 2013). After the dialysis membrane and biomass

had been removed, the surface pH of the agar was measured at specific intervals across the diameter of the plate using an Orion 3 Star benchtop pH meter (Thermo Fisher Scientific, Loughborough, UK) fitted with a flat tip electrode (VWR International, Lutterworth, England, UK).

Examination of biominerals produced in the presence of uranium

Secondary mineral formation in colonies grown with $UO_2(NO_3)_2$ and G2P was examined using light and scanning electron microscopy. Five-mm diameter cores were cut from the margins of fungal colonies grown for 30 days using a sterile cork borer and fixed in 2.5%(v/v) triple distilled glutaraldehyde in 5 mM 1,4-piperazine N,N′ bis (2-ethane sulphonic acid) (PIPES) buffer, pH 6.5, for at least 24 h at room temperature. The pH of 5 mM PIPES was adjusted using 1 M NaOH using a Corning pH meter 120 (Corning, NY 14831, USA). After fixation, samples were rinsed twice in 5 mM PIPES buffer, pH 6.5 (15 min per rinse) and then dehydrated through a graded ethanol series (50–100% (v/v), 15 min per step). Samples were then critical point dried using a liquid CO_2 BAL-TEC CPD 0.30 critical point dryer (BAL-TEC, Canonsburg, USA) and subsequently mounted on aluminium stubs using carbon adhesive tape and stored in a desiccator at room temperature. Prior to electron microscopy, samples were coated with 25 nm Au/Pd using a Cressington 208HR sputter coater and examined using a Philips XL30 environmental scanning electron microscope (ESEM) (Philips XL 30 ESEM FEG) operating at an accelerating voltage of 15kV. Secondary minerals formed on the fungal hyphae were examined for elemental composition using EDXA before Au/Pd coating the samples in order to exclude the Au/Pd peak which overlaps P/Cl peaks. Spectra were acquired using a Phoenix EDXA analysis system embedded within the environmental scanning electron microscope (Philips XL30 ESEM FEG) operating at an accelerating voltage of 20 kV. Samples were also ground into a fine powder using a mortar and pestle and used for X-ray mapping to investigate element location within the secondary minerals and biomass. X-ray powder diffraction was used to identify the secondary minerals produced. Diffraction patterns were recorded from 3 to 60° 2-θ using Ni-filtered Cu K-alpha radiation, counting for 300 s per 0.0167° step on a Panalytical X-pert Pro diffractometer using a X-celerator position sensitive detector. Mineral phases were identified by reference to patterns in the International Centre for Diffraction Data Powder Diffraction File.

Geochemical model PHREEQC

Geochemical software [PHREEQC, Ver. 3 (Parkhurst and Appelo, 2013)] was used to calculate the chemical equilibria of chemical and mineral species of uranium, phosphorus and oxalate to produce a geochemical model for the biotransformation of uranyl phosphate. The results are shown as predominance diagrams realized with PHREEPLOT, the graphic supporting software for PHREEQC (Smith *et al*., 2001; Charlton and Parkhurst, 2011; Parkhurst and Appelo, 2013). The available MINTEQ v4 database was integrated with critically selected stability constants of metal-oxalate complexes taken from the database of the National Institute of Standards and Technology, Ver. 8 (Smith *et al*., 2001). Thermodynamic data of uranyl phosphate, used for calculation of the predominance diagrams, are from Kalin and colleagues (2004). Total concentrations for U and P in the system were assumed to be 10 mM, and 30 mM for oxalate, the latter value taking account of measurements of oxalic acid excreted by *A. niger* after 12 days incubation in MCD and measured by high-performance liquid chromatography (results not shown).

Statistical analysis

R elaboration and programming software, version 3.0.2 (The R Foundation for Statistical Computing) and SIGMAPLOT, version 12.0 were used to perform statistical analyses. One-way analysis of variance tests on means were performed for dry weight, diametric growth and surface pH. At least three replicate determinations were used in all experiments.

Acknowledgements

We gratefully acknowledge the help of Mr Martin Kierans (Electron Microscopy, Central Imaging Facility, Centre for Advanced Scientific Technologies, College of Life Sciences, University of Dundee, Dundee, DD1 5EH, UK) for assistance with scanning electron microscopy. We thank David Parkhurst (USGS, Denver, CO, USA) and David Kinniburgh (BGS, Wallingford, UK) for their support in the thermodynamic calculations and their graphical display using PHREEQC and PHREEPLOT respectively. Stephen Hillier, Helen Pendlowski and Nia Gray acknowledge support of the Scottish Government's Rural and Environment Science and Analytical Services Division (RESAS).

References

Abd-Alla, M.H. (1994) Use of phosphorus by *Rhizobium leguminosarum* biovar viceae phosphatases. *Biol Fertil Soil* **18:** 216–218.

Aleksieva, P., Spasova, D., and Radoevska, S. (2002) Acid phosphatase distribution and localization in the Fugus *Humicola lutea*. *Z Naturforsch [C]* **58:** 239–243.

Andres, Y., MacCordick, H.J., and Hubert, J.C. (1993) Adsorption of several actinide (Th, U) and lanthanide (La, Eu, Yb) ions by *Mycobacterium smegmatis*. *Appl Microbiol Biotechnol* **39:** 413–417.

Andres, Y., MacCordick, H.J., and Hubert, J.C. (1994) Binding sites of sorbed uranyl ion in the cell wall of *Mycobacterium smegmatis*. *FEMS Microbiol Lett* **115:** 27–32.

Aseri, G.K., Jain, N., and Tarafder, J.C. (2009) Hydrolysis of organic phosphate forms by phosphatase and phytase producing fungi of arid and semi- arid soils of India. *Am Eurasian J Agric Environ Sci* **5:** 564–570.

Bonthrone, K.M., Basnakova, G., Lin, F., and Macaskie, L.E. (1996) Bioaccumulation of nickel by intercalation into polycrystalline hydrogen uranyl phosphate deposited via an enzymatic mechanism. *Nat Biotechnol* **14:** 635–638.

Charlton, S.R., and Parkhurst, D.L. (2011) Modules based on the geochemical model PHREEQC for use in scripting

and programming languages. *Comput Geosci* **37:** 1653–1663.
Fomina, M., Charnock, J.M., Hillier, S., Alvarez, R., and Gadd, G.M. (2007a) Fungal transformations of uranium oxides. *Environ Microbiol* **9:** 1696–1710.
Fomina, M., Podgorsky, V.S., Olishevska, S.V., Kadoshnikov, V.M., Pisanska, I.R., Hillier, S., and Gadd, G.M. (2007b) Fungal deterioration of barrier concrete used in nuclear waste disposal. *Geomicrobiol J* **24:** 643–653.
Fomina, M., Charnock, J.M., Hillier, S., Alvarez, R., Francis Livens, F., and Gadd, G.M. (2008) Role of fungi in the biogeochemical fate of depleted uranium. *Curr Biol* **18:** 375–377.
Fowle, D.A., Fein, J.B., and Martin, A.M. (2000) Experimental study of uranyl adsorption onto *Bacillus subtilis*. *Environ Sci Technol* **34:** 3737–3741.
Francis, A.J., Gillow, J.B., Cleveland, J.D., Harris, R., Beveridge, T.J., and Papenguth, H.W. (2004) Uranium association with halophilic and non-halophilic bacteria and archaea. *Radiochim Acta* **92:** 481–488.
Gadd, G.M. (2004) Microbial influence on metal mobility and application for bioremediation. *Geoderma* **122:** 109–119.
Gadd, G.M. (2007) Geomycology: biogeochemical transformations of rocks, minerals, metals and radionuclides by fungi, bioweathering and bioremediation. *Mycol Res* **111:** 3–49.
Gadd, G.M. (2010) Metals, minerals and microbes: geomicrobiology and bioremediation. *Microbiol* **156:** 609–643.
Gadd, G.M., and Fomina, M. (2011) Uranium and fungi. *Geomicrobiol J* **28:** 471–482.
George, T.S., Richardson, A.E., Gregory, P.J., and Simpson, R.J. (2007) Differential interaction of phytase proteins (PhyA) from *Aspergillus niger* and *Peniophora lycii* with soil particles has implications for mineralisation of phytate in soil. *Soil Biol Biochem* **39:** 793–803.
Gibson, B.R., and Mitchell, D.T. (2005) Phosphatases of ericoid mycorrhizal fungi: kinetic properties and the effect of copper on activity. *Myco Res* **109:** 478–486.
Gorman-Lewis, D., Elias, P.E., and Fein, J.B. (2005) Adsorption of aqueous uranyl complexes onto *Bacillus subtilis* cells. *Environ Sci Technol* **39:** 4906–4912.
Gorman-Lewis, D., Burns, P.C., and Fein, J.B. (2008) Review of uranyl mineral solubility measurements. *J Chem Thermodyn* **40:** 335–352.
Greenwood, A.J., and Lewis, D.H. (1977) Phosphatases and the utilisation of inositol hexaphosphate by soil yeasts of the genus *Cryptococcus*. *Soil Biol Biochem* **9:** 161–166.
Guibal, E., Roulph, C., and Lecloirec, P. (1995) Infrared spectroscopic study of uranyl biosorption by fungal biomass and materials of biological origin. *Environ Sci Technol* **29:** 2496–2503.
Kalin, M., Wheeler, W.N., and Meinrath, G. (2004) The removal of uranium from mining waste water using algal/microbial biomass. *J Environ Radioact* **78:** 151–177.
Krueger, S., Olson, G.J., Johnsonbaugh, D., and Beveridge, T.J. (1993) Characterization of the binding of gallium, platinum, and uranium to *Pseudomonas fluorescens* by small-angle X-ray scattering and transmission electron microscopy. *Appl Environ Microbiol* **59:** 4056–4064.
Kulkarni, S., Ballal, A., and Apte, S.K. (2013) Bioprecipitation of uranium from alkaline waste solutions using recombinant *Deinococcus radiodurans*. *J Hazard Mater* **262:** 853–861.
Lloyd, J.R., and Gadd, G.M. (2011) The geomicrobiology of radionuclides. *Geomicrobiol J* **28:** 383–386.
Lovley, D.R., and Phillips, E.J.P. (1992) Bioremediation of uranium contamination with enzymatic uranium reduction. *Environ Sci Technol* **26:** 2228–2234.
Lovley, D.R., Roden, E.E., Phillips, E.J.P., and Woodward, J.C. (1993) Enzymatic iron and uranium reduction by sulfate-reducing bacteria. *Mar Geol* **113:** 41–53.
Macaskie, L.E., Empson, R.M., Cheetham, A.K., Grey, C.P., and Skarnulis, A.J. (1992) Uranium bioaccumulation by a *Citrobacter* sp. as a result of enzymically mediated growth of polycrystalline HUO_2PO_4. *Science* **257:** 782–784.
Macaskie, L.E., Jeong, B.C., and Tolley, M.R. (1994) Enzymically accelerated biomineralization of heavy metals: application to the removal of americium and plutonium from aqueous flows. *FEMS Microbiol Rev* **14:** 351–367.
Macaskie, L.E., Bonthrone, K.M., Yong, P., and Goddard, D.T. (2000) Enzymically mediated bioprecipitation of uranium by a *Citrobacter* sp.: a concerted role for exocellular lipopolysaccharide and associated phosphatase in biomineral formation. *Microbiol* **146:** 1855–1867.
Markovic, M., and Pavkovic, N. (1983) Solubility and equilibrium constants of uranyl(2+) in phosphate solutions. *Inorg Chem* **22:** 978–982.
Markovic, M., Pavkovic, N., and Pavkovic, N.D. (1988) Precipitation of $NH_4UO_2PO_4{\cdot}3H_2O$ – solubility and structural comparison with alkali uranyl(2+) phosphates. *J Res Nat Bur Stand* **93:** 557–563.
Newsome, L., Morris, K., and Lloyd, J.R. (2014) The biogeochemistry and bioremediation of uranium and other priority radionuclides. *Chem Geol* **363:** 164–184.
Parkhurst, D.L., and Appelo, C.A.J. (2013). Description of input and examples for PHREEQC version 3 – A computer program for speciation, batch-reaction, one-dimensional transport, and inverse geochemical calculations. U.S. Geological Survey Techniques and Methods, Book 6, 43: 497.
Paterson-Beedle, M., Readman, J.E., Hriljac, J.A., and Macaskie, L.M. (2010) Biorecovery of uranium from aqueous solutions at the expense of phytic acid. *Hydrometallurgy* **104:** 524–528.
Rajeshkumar, J., and Ilyas, M.H.M. (2011) Production of phosphatase by mutated fungal strains. *Int Multidiscipli Res J* **5:** 23–29.
Ray, A.E., Bargar, J.R., Sivaswamy, V., Dohnalkova, A.C., Fujita, Y., Peyton, B.M., and Magnuson, T.S. (2011) Evidence for multiple modes of uranium immobilization by an anaerobic bacterium. *Geochim Cosmochim Acta* **75:** 2684–2695.
Rhee, Y.J., Hillier, S., and Gadd, G.M. (2012) Lead transformation to pyromorphite by fungi. *Curr Biol* **22:** 237–241.
Rhee, Y.J., Hillier, S., Pendlowski, H., and Gadd, G.M. (2014a) Pyromorphite formation in a fungal biofilm community growing on lead metal. *Environ Microbiol* **16:** 1441–1451.
Rhee, Y.J., Hillier, S., Pendlowski, H., and Gadd, G.M. (2014b) Fungal transformation of metallic lead to pyromorphite in liquid medium. *Chemosphere* **113:** 17–21.

Sivaswamy, V., Boyanov, M.I., Peyton, B.M., Viamajala, S., Gerlach, R., Apel, W.A., Sani, R.K., Dohnalkova, A., Kemner, K.M., and Borch, T. (2011) Multiple mechanisms of uranium immobilization by *Cellulomonas* sp. strain ES6. *Biotechnol Bioeng* **108:** 264–276.

Smith, R.M., Martell, A.E., and Motekaitis, R.J. (2001) *NIST Critically Selected Stability Constants of Metal Complexes Database*. Gaithersburg, MD, USA: NIST. NIST Standard Reference Database 46, version 6.0.

Suzuki, Y., and Banfield, J.F. (1999) Geomicrobiology of uranium. In *Reviews in Mineralogy and Geochemistry*. Redfern, S.A.T., and Carpenter, M.A. (eds). Washington, DC, USA: Mineralogical Society of America, pp. 393–432. Rev Mineral Geochem 38.

VanHaverbeke, L., Vochten, R., and VanSpringel, K. (1996) Solubility and spectrochemical characteristics of synthetic chernikovite and meta-ankoleite. *Mineral Mag* **60:** 759–766.

Vogel, K., and Hinnen, A. (1990) The yeast phosphatase system. *Mol Microbiol* **12:** 2013–2017.

Wei, Z., Liang, X., Pendlowski, H., Hillier, S., Suntornvongsagul, K., Sihanonth, P., and Gadd, G.M. (2013) Fungal biotransformation of zinc silicate and sulfide mineral ores. *Environ Microbiol* **15:** 2173–2186.

Yadav, R.S., and Tarafdar, J.C. (2003) Phytase and phosphatases producing fungi in arid and semi-arid soils and their efficiency in hydrolyzing different organic P. *Soil Biol Biochem* **35:** 745–751.

Yang, J., and Volesky, B. (1999) Modeling of the uranium-proton ion exchange in biosorption. *Environ Sci Technol* **33:** 4079–4085.

Yong, P., and Macaskie, L.M. (1995) Enhancement of uranium bioaccumulation by a *Citrobacter* sp. via enzymically-mediated growth of polycrystalline $NH_4UO_2PO_4$. *J Chem Technol Biotechnol* **63:** 101–108.

Yong, P., and Macaskie, L.M. (1998) Bioaccumulation of lanthanum, uranium and thorium, and use of a model system to develop a method for the biologically-mediated removal of plutonium from solution. *J Chem Technol Biotechnol* **71:** 15–26.